JOURNAL OF SOLID STATE CHEMISTRY 100, 37–48 (1992)

The Crystal Structure and Magnetic Properties of $SrLaFeSnO_6$ and $SrLaNiSbO_6$

M. P. ATTFIELD, P. D. BATTLE,* AND S. K. BOLLEN

Inorganic Chemistry Laboratory, South Parks Road, Oxford, OX1 3QR, England

T. C. GIBB*

School of Chemistry, The University, Leeds, LS2 9JT, England

AND R. J. WHITEHEAD

Physics Department, Durham University Science Laboratories, South Road, Durham, DH1 3LE, England

Received November 18, 1991; accepted February 25,1992

The crystal and magnetic structures of the perovskite-related materials $SrLaFeSnO_6$ and $SrLaNiSbO_6$ have been refined using neutron diffraction data collected at room temperature and 1.7 K. $SrLaFeSnO_6$ adopts the orthorhombic space group *Pbnm* with disordered Sr/La and Fe/Sn cations and is magnetically ordered as a G-type antiferromagnet at 1.7 K. $SrLaNiSbO_6$ differs in that a partial order of the Ni and Sb cations results in the space group $P2_1/n$ and a Type I antiferromagnetic structure. The magnetic susceptibility shows a maximum at 39 and 26 K, respectively, but there is a significant difference between the field-cooled and zero-field-cooled susceptibility above these temperatures. This effect persists to at least 250 K in $SrLaFeSnO_6$. An explanation is developed in terms of magnetic clusters which increase in size with decreasing temperature until a long-range ordered structure is finally achieved.

Introduction

The crystal structure and magnetic properties of perovskite-related materials with the formula $ABB'O_6$ or $AA'BB'O_6$ depend upon the size and electronic structure of the transition metal cations *B* and *B'*. If the two species are of similar size and charge they are likely to be distributed over the 6-coordinate sites in a disordered manner, otherwise they may order in an alternate arrangement, thus increasing the size of the unit cell. The presence of cation disorder on the *B* sublattice has been shown to give rise to unusual magnetic behavior, for example, competing superexchange interactions lead to spin-glass behavior in Sr_2FeRuO_6 and $BaLaNiRuO_6$ (*1*), whereas the magnetically more dilute compound Sr_2YRuO_6, which has an ordered arrangement of Y^{3+} and Ru^{5+} cations, orders antiferromagnetically at low temperatures (*2*). We have recently found

* To whom correspondence should be addressed.

0022-4596/92 $5.00

spin-glass behavior in Sr_2FeTiO_{6-y}, where the cause is spin frustration from the multiple electronic states of the Fe cations (*3*). Moreover, Sr_2FeNbO_6, which is both magnetically dilute and apparently structurally disordered (*4*), behaves as a spin glass, even though the concentration of magnetic ions (Fe^{3+}) is considerably in excess of the percolation threshold (30.7%) for a simple cubic lattice.

We have now studied two more magnetically dilute perovskites, $SrLaFeSnO_6$ and $SrLaNiSbO_6$, in order to investigate further the correlation between structural disorder and magnetic behavior. We show that these two compounds, in which the diamagnetic, 6-coordinate cation has a $4d^{10}$ electron configuration in contrast to the $4d^0$ configuration of Nb^{5+}, behave differently from each other and also from Sr_2FeNbO_6.

Experimental

Accurately weighed amounts of spectroscopic grade Fe_2O_3, SnO_2, La_2O_3, and $SrCO_3$ with stoichiometric ratios appropriate for $SrLaFeSnO_6$ were ground together in a ball mill, pressed into a pellet, and fired in a platinum crucible at temperatures ranging from 1200 to 1400°C with several intermediate grindings for a total time of between 20 and 30 days before finally quenching in air. The brown-ochre product was reproducible despite a reluctance to sinter at 1400°C. $SrLaNiSbO_6$ was prepared in a similar way, using Sb_2O_3 as a source of antimony. The reaction mixture was heated for 8 days in an alumina crucible at a maximum temperature of 1200°C and a gray-green product formed. In both cases the progress of the reaction was monitored by X-ray powder diffraction recorded with a Philips diffractometer using nickel-filtered CuK_α radiation. The X-ray patterns of the final products were consistent with their being perovskite-related phases.

Neutron powder diffraction data were collected on both compounds at room temperature using the diffractometer D1a at ILL Grenoble. The angular range $6 < 2\theta < 144°$ was scanned with a step size of 0.05° using a mean neutron wavelength of 1.9127 Å. The samples were contained in 16 mm diameter vanadium cans. Further data sets were collected with the samples held at a temperature of 1.7 K in an Al-tailed cryostat.

The magnetic susceptibilities of Sr $LaFeSnO_6$ and $SrLaNiSbO_6$ were measured in the temperature range $4.2 < T < 300$ K with an Oxford Instruments Faraday balance in a magnetic field of 0.1 T and a field gradient of 1 Tm^{-1}. Measurements were made after cooling the sample in zero field and after cooling in the measuring field.

Mössbauer data were collected in the same temperature range for $SrLaFeSnO_6$ using $^{57}Co/Rh$ and $^{119m}Sn/CaSnO_3$ source matrices held at room temperature.

Results

(*i*) *Neutron Diffraction*

All the neutron powder diffraction profiles collected in the experiments described above were analyzed by the Rietveld profile analysis technique (*5, 6*) using the following neutron scattering lengths: $b_{Sr} = 0.69$, $b_{La} = 0.83$, $b_{Fe} = 0.95$, $b_{Ni} = 1.03$, $b_{Sn} = 0.61$, $b_{Sb} = 0.56$, and $b_O = 0.58 \times 10^{-12}$ cm. The background level was estimated by interpolation between regions where there were no Bragg peaks, and the latter were assumed to have a pseudo-Voigtian line profile.

(*a*) *The crystal structure of $SrLaFeSnO_6$ at room temperature.* The neutron powder diffraction data collected on $SrLaFeSnO_6$ at room temperature were consistent with the adoption of a distorted perovskite-like structure in the orthorhombic space group *Pbnm* with unit cell parameters of ca. $\sqrt{2}a_p \times \sqrt{2}a_p \times 2a_p$, where a_p is the unit cell parameter of a simple cubic perovskite.

TABLE I

STRUCTURAL PARAMETERS OF $SrLaFeSnO_6$ AT ROOM TEMPERATURE (SPACE GROUP *Pbnm*)

Atom	Site	x	y	z	B_{iso} (Å^2)
Sr/La	4c	0.0042(6)	0.0226(2)	¼	0.96(2)
Fe/Sn	4a	½	0	0	0.21(2)
O1	8d	0.2796(3)	0.2795(4)	0.0344(2)	0.71(3)
O2	4c	0.9301(7)	0.4892(4)	¼	0.79(6)

Note. a = 5.6555(1), b = 5.6544(1), c = 7.9909(2) Å.

TABLE II

BOND LENGTHS (Å) AND BOND ANGLES (deg) FOR $SrLaFeSnO_6$ AT ROOM TEMPERATURE

Fe/Sn–O1	2.031(3) × 2	Sr/La–O1	2.739(5) × 2
Fe/Sn–O2	2.033(5) × 2	Sr/La–O1	2.834(5) × 2
Fe/Sn–O2	2.037(5) × 2	Sr/La–O1	2.520(5) × 2
		Sr/La–O2	2.463(6)
Average Fe/Sn–O	2.034	Sr/La–O2	2.671(6)
Shortest O–O contact: O1—O2	2.863(6)		
O1–Fe/Sn–O1	91.06	Fe/Sn–O1–Fe/Sn	159.4
O1–Fe/Sn–O2	90.55	Fe/Sn–O2–Fe/Sn	157.3
O1′–Fe/Sn–O2	90.01		

This space group does not permit ordering of two different elements over the 6-coordinate B sites and our refinements were therefore carried out with a disordered arrangement of Fe and Sn on the octahedral sites. Similarly, the La^{3+} and Sr^{2+} cations were disordered over the A sites. Refinement of 11 atomic parameters and the usual profile parameters using 142 Bragg peaks resulted in the structural parameters listed in Table I and the profile fit in Fig. 1. The final integrated intensity agreement factor was R_I = 2.5% and the weighted profile factor was R_{wpr} = 4.8%. The most important bond lengths and angles are listed in Table II.

(*b*) *The crystal structure of* $SrLaNiSbO_6$ *at room temperature.* $SrLaNiSbO_6$ has been described previously (*7*) as a cubic perovskite, but our data indicated a lower symmetry. Attempts to refine the crystal structure in space group *Pbnm* were unsuccessful and we therefore lowered the symmetry to monoclinic, space group $P2_1/n$. This space group does permit ordering of the Ni^{2+} and Sb^{5+} cations over the 6-coordinate sites of the perovskite structure, although the Sr^{2+} and La^{3+} cations remain disordered on the A sites. Subsequent refinements of eighteen atomic parameters and the usual profile parameters using 262 Bragg reflections led to the agreement factors R_I = 3.1%, R_{wpr} = 5.4%. The Ni/Sb distribution over the two crystallographically distinct B sites was allowed to vary, with the constraint that the 1 : 1 composition ratio was maintained; the isotropic temperature factors of these two

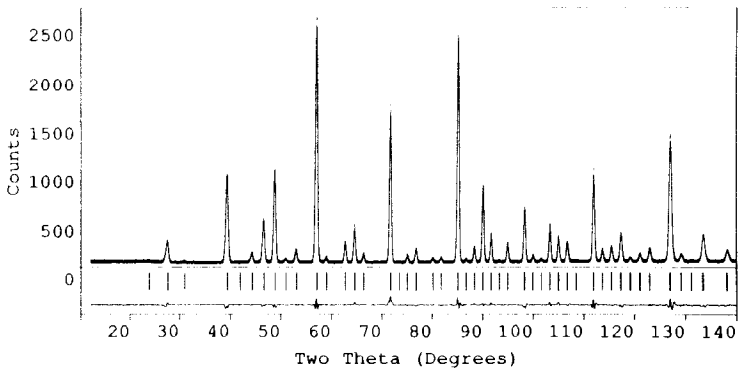

FIG. 1. The observed (....), calculated (—), and difference neutron powder diffraction profiles of $SrLaFeSnO_6$ at room temperature. Reflection positions are marked.

TABLE III

STRUCTURAL PARAMETERS OF $SrLaNiSbO_6$ AT ROOM TEMPERATURE (SPACE GROUP $P2_1/n$)

Atom	Site	x	y	z	B_{iso} (Å^2)
Sr/La	4e	0.0052(6)	0.0210(4)	0.751(1)	0.71(2)
B^a	2d	$\frac{1}{2}$	0	0	0.20(2)
B'^b	2c	0	$\frac{1}{2}$	0	0.20(2)
O1	4e	0.2748(8)	0.2753(10)	0.9708(7)	0.48(11)
O2	4e	0.2797(10)	0.2877(12)	0.5426(6)	0.84(13)
O3	4e	0.9383(7)	0.4933(5)	0.7415(8)	0.46(7)

Note. a = 5.6402(2), b = 5.6254(2), c = 7.9581(3) Å, β = 90.06°.

[a] Site B fractional occupancy: 0.10(1) Ni, 0.90(1) Sb.

[b] Site B' fractional occupancy: 0.90(1) Ni, 0.10(1) Sb.

sites were constrained to be equal. The final values of the refined parameters are listed in Table III, with the corresponding bond lengths and bond angles in Table IV. The observed and calculated neutron diffraction patterns are shown in Fig. 2. It is clear from this figure that our sample of $SrLaNiSbO_6$ contains a small amount of a second phase, which our initial examination by X-ray diffraction failed to detect.

(*c*) *The crystal and magnetic structures of* $SrLaFeSnO_6$ *at 1.7 K.* In comparison to those collected at room temperature, the low-temperature diffraction data on

TABLE IV

BOND LENGTHS (Å) AND BOND ANGLES (deg) FOR $SrLaNiSbO_6$ AT ROOM TEMPERATURE

B–O1	2.016(9) × 2	B'–O1	2.013(9) × 2
B–O2	2.007(10) × 2	B'–O2	2.069(10) × 2
B–O3	1.954(8) × 2	B'–O3	2.086(8) × 2
Average B–O 1.992		Average B'–O 2.056	
Shortest O–O contact: O2–O3 2.75(1)			
Sr/La–O1	Sr/La–O2		Sr/La–O3
2.72(1)	2.72(1)		2.99(1)
2.56(1)	2.42(1)		2.69(1)
2.83(1)	2.86(1)		2.51(1)
O1–B–O2	86.7	O1–B'–O2	89.4
O1–B–O3	89.2	O1–B'–O3	89.8
O2–B–O3	87.9	O2–B'–O3	87.3
B–O1–B'	162.5	B–O2–B'	155.5
B–O3–B'	160.0		

$SrLaFeSnO_6$ contained additional Bragg scattering indicative of the presence of long-range magnetic ordering. The angular distribution of this intensity suggested that this compound orders as a G-type antiferromagnet (*8*) with the atomic moments of the magnetic cations arranged as shown in Fig. 3. It must be remembered that, statistically, only half of the cation sites are magnetically active, the remainder being occupied by Sn^{4+}. We performed a simultaneous Rietveld refinement of the crystal and magnetic structures, using the free-ion form factor (*9*) of Fe^{3+} to describe the angular dependence of the magnetic scattering amplitude. There was no evidence of any change in the crystal symmetry between room temperature and 1.7 K. In addition to those parameters refined in the analysis of the room temperature crystal structure, we included the average ordered magnetic moment of the 6-coordinate cations. The final structural parameters are listed in Table V and the observed and calculated diffraction profiles are presented in Fig. 4. The average magnetic moment was found to be 1.47(2) μ_B per site, that is 2.94 μ_B per Fe^{3+} cation, aligned along the crystallographic z axis. There were no significant changes in the Fe/Sn–O bond distances between room temperature and 1.7 K. The agreement factors resulting from this experiment were R_I = 1.8%, R_{wpr} = 5.0%.

(*d*) *The crystal and magnetic structures of* $SrLaNiSbO_6$ *at 1.7 K.* Weak magnetic scattering was also visible at low 2θ angles in the diffraction pattern of $SrLaNiSbO_6$ taken at 1.7 K. However, the distribution of this additional scattering over the various Bragg reflections was very different from that seen in $SrLaFeSnO_6$, being similar to that observed previously (*10*) from the ordered perovskite Sr_2ErRuO_6. We therefore analyzed our data using the magnetic structure drawn in Fig. 5, which consists of two interpenetrating cation sublattices, B and B', with a different average ordered magnetic moment per cation for each sublattice.

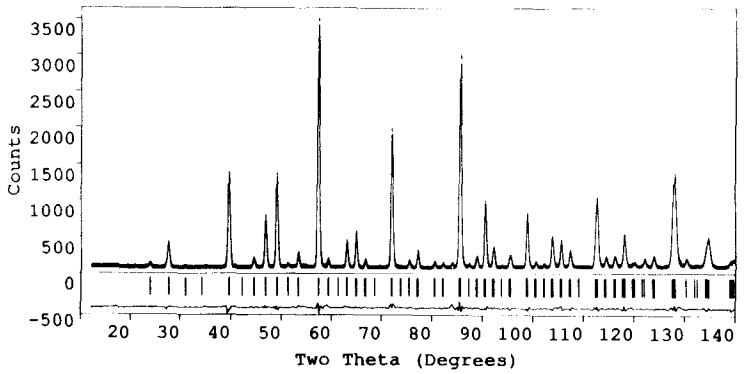

FIG. 2. The observed (....), calculated (—), and difference neutron powder diffraction profiles of $SrLaNiSbO_6$ at room temperature. Reflection positions are marked.

Preliminary refinements of the crystal structure indicated that no major change had occurred on cooling and the cation distribution over the sites B and B' was therefore held constant at the previously determined ratio during analysis of the low temperature data. Simultaneous refinement of the crystal and magnetic structures then resulted in the structural parameters listed in Table VI and the observed and calculated diffraction patterns drawn in Fig. 6, with agreement factors $R_I = 3.0\%$ and $R_{wpr} = 6.1\%$. The free-ion form factor of Ni^{2+} (*9*) was used in the data analysis. The magnetic moments refined to values of $-0.03(4)\ \mu_B$ for site B and $1.38(5)\ \mu_B$ for site B', directed along the x axis; the latter corresponds to a moment of $1.53\ \mu_B$ per Ni^{2+} ion.

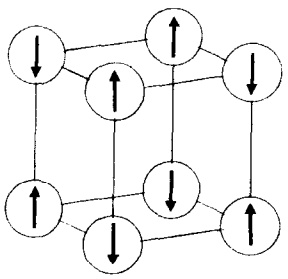

FIG. 3. The G-type antiferromagnetic structure, as found in $SrLaFeSnO_6$. Only the 6-coordinate cations in a simple cubic perovskite cell are shown.

(ii) Magnetic Susceptibility

The molar susceptibility of $SrLaFeSnO_6$ is plotted as a function of temperature in Fig. 7. The data taken after cooling in zero applied field (zfc) show a maximum at ca. 38 K and suggest that this compound is antiferromagnetic at low temperatures, consistent with the neutron diffraction data described above. However, the susceptibility does not show a Curie–Weiss behavior in any part of the measured temperature range, and moreover close examiantion shows some evidence for significant magnetic interactions up to ca. 200 K, in agreement with the Mössbauer data referred to below. Furthermore, the field-cooled (fc) data show a very different temperature dependence and diverge significantly from the zfc data below ca. 250 K. This behavior, which is discussed in more detail below, suggests that complex magnetic interactions are occurring at all temperatures below 250 K in $SrLaFeSnO_6$. The molar magnetic susceptibility of $SrLaNiSbO_6$ is plotted as a function of temperature in Fig. 8. Both the zfc and fc curves show a maximum at ca. 26 K,

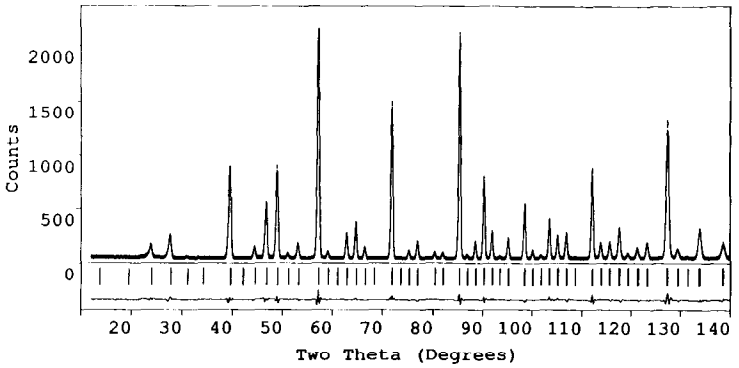

FIG. 4. The observed (....), calculated (—), and difference neutron powder diffraction profiles of $SrLaFeSnO_6$ at 1.7 K. Reflection positions are marked.

but they do not coincide at temperatures below 60 K. Comparison of Figs. 7 and 8 suggests that the two compounds behave in similar ways, although the deviation from classical Néel antiferromagnetism is more marked in the case of $SrLaFeSnO_6$. Indeed, $SrLaNiSbO_6$ obeys a Curie–Weiss Law above ca. 200 K with $\mu_{eff} = 2.83\ \mu_B$ per Ni^{2+} ion.

(*iii*) *Mössbauer Spectroscopy*

While the neutron data established that there is no long-range cation ordering in $SrLaFeSnO_6$, there still remains the possibility of short-range ordering. This possibility can be investigated by Mössbauer spectroscopy, which observes individual atomic environments. A convincing measurement of cation disorder was obtained from the magnetic hyperfine interactions. The ^{57}Fe resonance shows a magnetic hyperfine interaction below ca. 210 K, which is accompanied by a transferred hyperfine interaction in the ^{119m}Sn resonance. The hyperfine effects in both resonances are complicated by relaxation effects, and these results will be the subject of a separate paper (*11*). However, the dynamic processes freeze out at low temperatures. The magnetic splitting of the ^{119m}Sn resonance at 4.2 K is illustrated in Fig. 9a. The Sn^{4+} cation has no intrinsic spin moment, but a near-neighbor Fe^{3+} cation can induce a transferred hyperfine field at the Sn nucleus (*12*). A substitutional Sn atom in a rare-earth orthoferrite such as $LaFeO_3$ shows a large hyperfine field with a flux density of some 25 T, which arises from the six near-neighbor Fe cations with parallel spins which thereby reinforce each other. Replacing one Fe cation with a diamagnetic cation such as Al or Ga reduces the transferred hyperfine field in proportion. In a solid solution a number of superimposed hyperfine fields can be observed representing a summation of the different near-neighbor groupings. The binomial probabilities for zero to six near-neighbor Fe^{3+} cations in a Fe/Sn disordered system are 0.0156, 0.0938, 0.2344, 0.3125, 0.2344, 0.0938, and 0.0156,

TABLE V

STRUCTURAL PARAMETERS OF $SrLaFeSnO_6$ AT 1.7 K (SPACE GROUP *Pbnm*)

Atom	Site	x	y	z	B_{iso} (Å^2)
Sr/La	4c	0.0055(6)	0.0262(2)	¼	0.64(2)
Fe/Sn	4a	½	0	0	0.15(2)
O1	8d	0.2811(3)	0.2813(3)	0.0355(2)	0.50(3)
O2	4c	0.9287(7)	0.4870(4)	¼	0.63(6)

Note. a = 5.6471(1), b = 5.6506(1), c = 7.9810(2) Å.

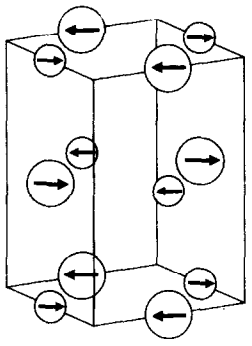

FIG. 5. The magnetic structure proposed for $SrLaNiSbO_6$, consisting of two interpenetrating sublattices with a different atomic moment associated with each.

respectively. The predicted ^{119m}Sn spectrum, assuming a flux density of 25 T for 6 Fe^{3+} neighbors with the other flux densities in linear proportion and a linewidth of 1.2 mm s^{-1}, is shown in Fig. 9c. The magnetic moments used were $\mu_g = -1.0461\ \mu_N$, $\mu_e/\mu_g = 0.645$ with the gamma-ray energy as 23.871 keV. The quadrupole interaction is too small to have any significant effect on the spectrum and has been ignored. The overall distribution of fields corresponds well with the experimental data apart from the lack of resolution in the latter. It is clear that the distribution of Fe about the Sn must be close to random, and that all Fe near neighbors have almost parallel spins. In particular, the small number of Sn cations with a near-zero hyperfine field is very small as shown by the very weak central feature. The broadening seen experimentally probably arises from a combination of local lattice relaxation effects, as the transferred hyperfine interaction will be very sensitive to bond distances and bond angles, and some degree of spin misalignment due to the complexity of the spin interactions in the disordered system. The curve in Fig. 9b was obtained by introducing an additional broadening into each hyperfine line proportional to its displacement from the centroid, thereby simulating a distribution of hyperfine fields for each nominal near-neighbor combination. The agreement with experiment is quite good for such a simple model.

The high critical temperature observed in the Mössbauer spectra is also compatible with a disordered cation distribution in a lattice where the percolation threshold would be reached at 69.3% substitution by tin. Local cation clustering would magnetically isolate a significant proportion of the iron atoms even at low temperatures, and there is no evidence for this happening. All the magnetic atoms show a large hyperfine field at 78 K, characteristic of strong interatomic coupling. The relaxation effects seen at higher temperatures are clearly related to the behavior observed in the magnetic susceptibility data, but will be discussed in detail in a later paper.

TABLE VI

STRUCTURAL PARAMETERS OF $SrLaNiSbO_6$ AT 1.7 K (SPACE GROUP $P2_1/n$)

Atom	Site	x	y	z	B_{iso} (Å^2)
Sr/La	4e	0.0066(6)	0.0259(4)	0.252(1)	0.32(3)
B	2d	$\frac{1}{2}$	0	0	0.07(2)
B'	2c	0	$\frac{1}{2}$	0	0.07(2)
O1	4e	0.2901(12)	0.2815(15)	0.0413(6)	0.2(2)
O2	4e	0.2691(12)	0.2851(13)	0.4718(7)	0.7(2)
O3	4e	0.9341(9)	0.4928(7)	0.2523(11)	0.07(6)

Note. $a = 5.6313(3)$, $b = 5.6215(2)$, $c = 7.9494(3)$ Å, $\beta = 90.07°$.

Discussion

The crystal structure of $SrLaFeSnO_6$ is similar to that of other perovskite-related materials that have been studied previously, for example, La_2NiRuO_6 (*13*). The difference in size and effective charges between Fe^{3+} and Sn^{4+} is sufficiently small for them to occupy the 6-coordinate sublattice in a disordered manner. The results listed in Table II show that the oxide ions that surround the B site form an essentially regular octahedron, although it is important to remember

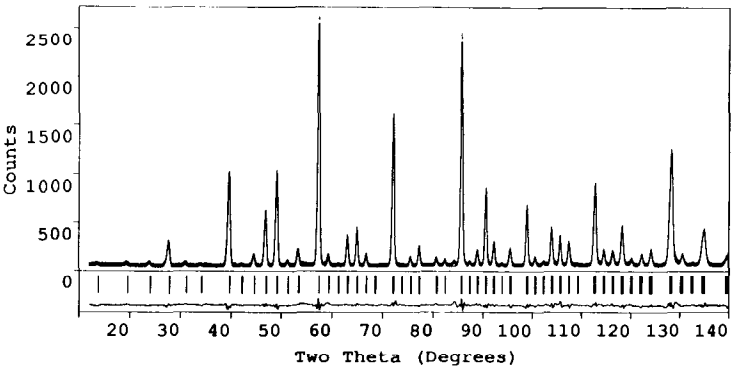

FIG. 6. The observed (....), calculated (—), and difference neutron powder diffraction profiles of $SrLaNiSbO_6$ at 1.7 K. Reflection positions are marked.

that a neutron diffraction experiment samples the average structure and gives no direct information on local atomic displacements. However, the values of the temperature factors in Table I are entirely reasonable for a mixed metal oxide, thus suggesting that any local displacements are small and hence that there is no significant short range order among the disordered cations. The disordered nature of the phase is confirmed by the ^{119m}Sn Mössbauer data. The transferred hyperfine interactions at the tin can only be explained in terms of a *random* distribution of Fe and Sn atoms on the *B*-sites. There is no evidence for clustering of tin atoms, or for any tendency to form a local alternation of cations. Both of these effects would significantly increase the central components in the spectrum, and this is not observed. The average Fe/Sn–O bond-length of 2.034 Å is as expected in the light of those found (*14*, *15*) in the related

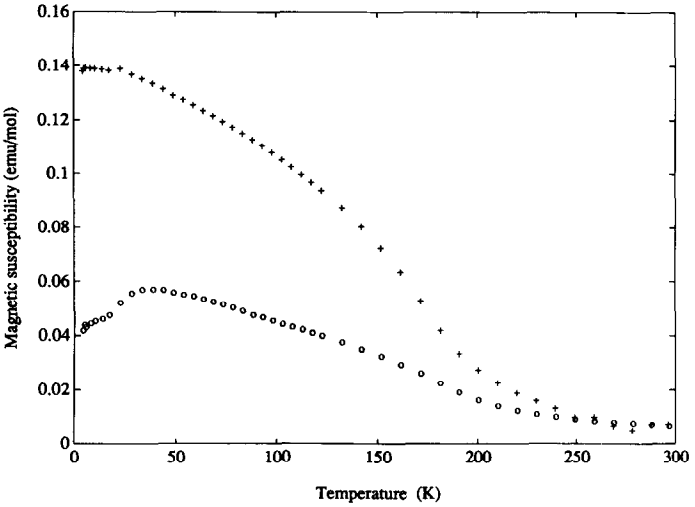

FIG. 7. The molar magnetic susceptibility of $SrLaFeSnO_6$ as a function of temperature: (○) after zero-field-cooling and (+) after cooling in the measuring field.

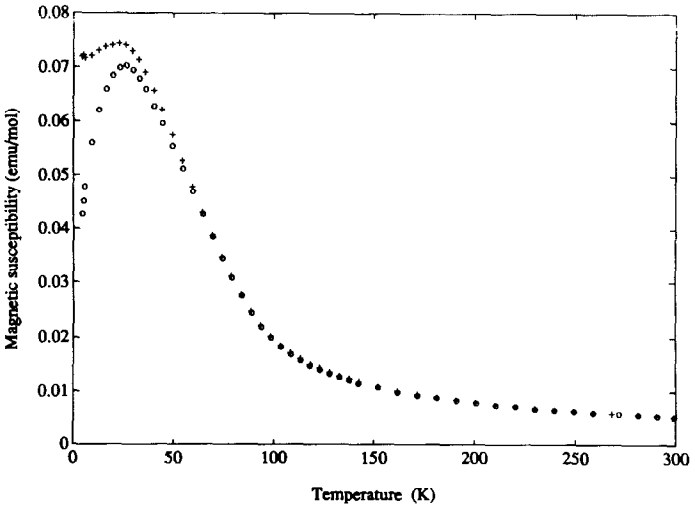

FIG. 8. The molar magnetic susceptibility of $SrLaNiSbO_6$ as a function of temperature: (○) after zero-field-cooling and (+) after cooling in the measuring field.

compounds $LaFeO_3$ and $CaSnO_3$ (2.006 and 2.062 Å respectively). The crystal structure of $SrLaNiSbO_6$ is more unusual in that it has a partially ordered arrangement of cations on the 6-coordinate sites. The difference in charge between Ni^{2+} and Sb^{5+} will be greater than between Fe^{3+} and Sn^{4+} in $SrLaFeSnO_6$, but not by the two units implied by the use of formal oxidation states. The move toward an ordered structure is more likely to be driven by the increased size difference between the two cations. The average length of the B–O bonds (Table IV) is similar to the value of 1.982 Å found for the Sb–O bonds in $SrLaCuSbO_6$ (*16*), whereas the mean B′–O bond length approaches that of 2.089 Å found for the Ni–O bond in NiO. It should be noted that the precision of our structure refinement of $SrLaNiSbO_6$ is lower than that associated with our description of $SrLaFeSnO_6$, possibly due in part to the presence of a small amount of impurity in the sample.

In a magnetically concentrated structure, G-type ordering leaves each cation antiferromagnetically coupled to six nearest neighbors at a distance a_p and ferromagnetically

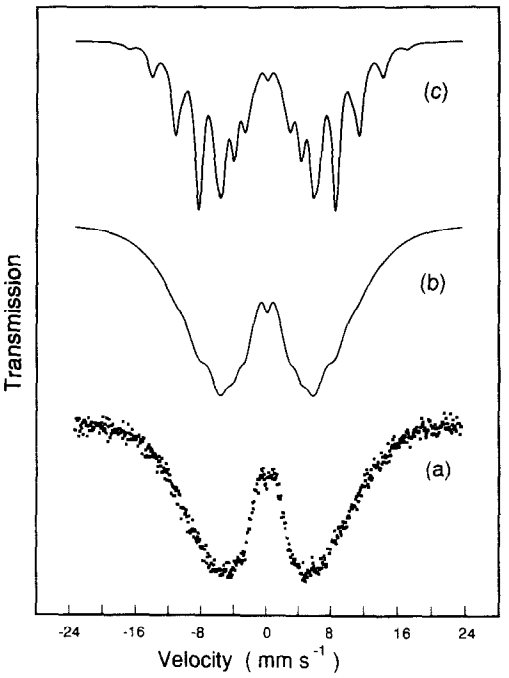

FIG. 9. The ^{119m}Sn Mössbauer spectrum of $SrLaFeSnO_6$ at 4.2 K: (a) experimental data, (b) simulated with additional broadening of the hyperfine fields, and (c) simulated without additional broadening of the hyperfine fields, as detailed in the text.

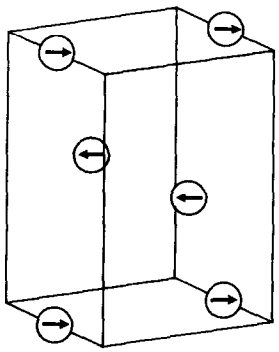

FIG. 10. The unit cell of a Type I antiferromagnet.

aligned with respect to 12 next-nearest neighbors (nnn) at a distance $\sqrt{2}a_p$. The adoption of a G-type structure, despite the fact that the nnn interaction is also inherently antiferromagnetic, shows that the nearest-neighbor coupling is dominant in $SrLaFeSnO_6$, although each Fe^{3+} ion will have between zero and six magnetically inactive nearest neighbors. It should be noted that the average ordered component of the magnetic moment per Fe^{3+} cation at 1.7 K is much lower than would have been expected in a fully ordered antiferromagnet (*17*).

The magnetic structure of $SrLaNiSbO_6$ at 1.7 K differs from that of $SrLaFeSnO_6$ in a manner which is consistent with the presence of long-range cation order in the former but not in the latter. The partial ordering reduces the number of magnetic nearest-neighbor pairs (separation a_p), whilst increasing the number of magnetic nnn pairs (separation $\sqrt{2}a_p$). The *B'* sublattice (80% Ni^{2+}) therefore adopts a Type I magnetic structure (Fig. 10) which favors antiferromagnetic coupling between cations a distance $\sqrt{2}a_p$ apart. Despite their low concentration, the Ni^{2+} cations on the *B* sublattice order in a similar arrangement, the nearest-neighbor superexchange between *B* and *B'* ensuring that the two interpenetrating Type I sub-structures are antiferromagnetically aligned, as drawn in Fig. 5. Superexchange coupling between 3rd nearest neighbors is too weak to play a role in determining the magnetic structure. The magnetic moment per Ni^{2+} ion on the *B'*-site is slightly lower than might have been expected and the ordered moment on the *B*-site is very small and has a large standard deviation associated with it. However, the observed magnetic Bragg intensity distribution cannot be accounted for using a collinear magnetic structure unless there is a small contribution from the *B*-site.

The magnetic susceptibilities of $SrLaFeSnO_6$ and $SrLaNiSbO_6$ show a most curious temperature dependence. At low temperatures the zero-field-cooled (zfc) susceptibility shows a maximum for both compounds, at 39 and 26 K, respectively, and this probably marks the onset of the long-range antiferromagnetism detected at 1.7 K in the neuutron diffraction experiments. However, in the temperature regime above the maximum the zfc and field-cooled (fc) data do not coincide, as they would for a simple Curie–Weiss paramagnet. $SrLaFeSnO_6$ can be thought of as belonging to the system $Sr_xLa_{1-x}Fe_{1-x}Sn_xO_3$ ($x = 0.5$, and it is therefore useful to consider the susceptibility data in the light of $LaFeO_3$. The latter compound orders as a G-type antiferromagnet (albeit with a weak ferromagnetic contribution) at a temperature of 750 K (*18*). It is therefore not surprising that significant short-range magnetic interactions are present in $SrLaFeSnO_6$ below 250 K. The magnetic concentration of the *B*-sites (50%) is much greater than the percolation limit (30.7%), and calculations (*11*) show that 87% of the Fe atoms in a fully disordered structure belong to a single bi-connected pathway which represents the magnetic "backbone" of the lattice. Of the remainder, more than 9% are connected to the backbone as "dangling ends," and only 1.56% are completely isolated with six Sn nn atoms. Magnetically isolated "clusters" as such are not significant. One would therefore expect to see a long-range ordered anti-

ferromagnet with a Néel temperature of the order of 300 K, and it is surprising that the susceptibility shows a maximum at such a low temperature.

We believe that, although the composition is well away from the percolation limit, the behavior of this compound can still be explained in terms of percolation theory and the growth of magnetic clusters. A similar situation has already been studied close to the percolation limit in $KMn_cMg_{1-c}F_3$ (*19*) and $KMn_cZn_{1-c}F_3$ (*20, 21*), both simple cubic antiferromagnets containing a $3d^5$ magnetic ion, i.e., very similar to the present instance. Cyrot (*22*) has developed a model for the behavior of frustrated spin glasses which involves the growth of blocks of coupled spins above the glass transition temperature. The size of the blocks increases with decreasing temperature until at some temperature T_G a block of infinite size is formed. The observation of Bragg peaks at 1.7 K proves that $SrLaFeSnO_6$ is not a spin glass, nor is the lattice truly frustrated. However, a model in which clusters of antiferromagnetically coupled spins develop at relatively high temperatures, and increase in size as the temperature is lowered, may be applicable in this case. A number of factors can be identified which are relevant. Although 87% of the Fe atoms are biconnected, there are nevertheless many regions in the lattice with a comparatively small number of pathways, so that thermal energy will break these easily. The Fe^{3+} ion is nominally an *S*-state ion, and as such will reorientate its magnetic moment readily in response to the local ligand-field effects caused by randomisation. Moreover, atoms with few nn Fe^{3+} ions will still have on average six nnn Fe^{3+} ions, and this enhancement of the significance of the nnn interactions may well introduce a certain degree of spin frustration. All of these effects will weaken the long-range ordering with increase in thermal energy, and lead to an increasing tendency for small clusters to decouple from the spin system. The high-temperature clusters are likely to carry an uncompensated magnetic moment, the orientation of which will be influenced by an external field, as is shown by the observed variation of susceptibility on cooling in a field and in zero field.

We thus begin to understand our data in terms of magnetic clusters which grow with decreasing temperature and form a cluster with an infinite backbone at 39 K. Clearly, not all spins are linked to this backbone at 1.7 K because the ordered magnetic moment per Fe^{3+} cation is too low, although some of this effect could be due to spin misalignment from local ligand-field effects. Many further experiments suggest themselves as a result of this simplistic explanation. It is clearly desirable to perform similar studies on samples having different Fe/Sn ratios, and to carry out neutron diffraction studies to monitor the variation in intensity of the magnetic Bragg peaks as a function of temperature. A Mössbauer study of the relaxation behavior of this spin system has already been carried out (*11*).

The magnetic behavior of $SrLaNiSbO_6$ is similar to that of $SrLaFeSnO_6$, although the difference between the fc and zfc susceptibilities is less marked and occurs over a narrower temperature range. This may well be because the degree of disorder is much lower in the former compound, and the temperature domain in which cluster formation occurs is considerably smaller; the system moves from a paramagnetic state to a long-range ordered state over a temperature range of only ca. 30 K. The transition begins at a lower absolute temperature because the principal magnetic superexchange is between cations separated by a distance $\sqrt{2}a_p$, rather than a_p. Furthermore, 6-coordinate Ni^{2+} has the electronic structure $t_{2g}^6e_g^2$ and hence there can be no significant π contribution to the superexchange, in contrast to Fe^{3+}, $t_{2g}^3e_g^2$. There are no other Ni^{2+} perovskites to provide a straightforward comparison with $SrLaNiSbO_6$ but it would

be interesting to study other samples in the series $Sr_{1+3x}La_{1-3x}Ni_{1-x}Sb_{1+x}O_6$ having different Ni/Sb ratios.

Finally we note that neither $SrLaFeSnO_6$ nor $SrLaNiSbO_6$ displays the same spin-glass behavior as was observed in Sr_2FeNbO_6. This may be due to the lowering of the vacant energy levels on the diamagnetic 6-coordinate cation, which enables these d^{10} cations to play a greater role in the magnetic superexchange. The magnetic properties of perovskites with more than one cation species on the octahedral sites are clearly very sensitive to changes in composition, a factor that we are presently studying in more depth.

Acknowledgments

We are grateful to Dr. J. K. Cockcroft for assistance during our visit to ILL, and to the SERC for financial support. The sample of $SrLaNiSbO_6$ was prepared by T. M. Frankcom.

Note added in proof. Figures 7 and 8 were inadvertently prepared with an incorrect numerical scale for the magnetic susceptibility. The values shown should be multiplied by a factor of 0.65. The discussion is not affected.

References

1. P. D. Battle, T. C. Gibb, C. W. Jones, and F. Studer, *J. Solid State Chem.* **78,** 281 (1989).
2. P. D. Battle and W. J. Macklin, *J. Solid State Chem.* **52,** 138 (1984).
3. T. C. Gibb, P. D. Battle, S. K. Bollen, and R. J. Whitehead, *J. Mater. Chem.*, **2,** 111 (1992).
4. R. Rodríguez, A. Fernández, A. Isalgué, J. Rodríguez, A. Labarta, J. Tejada, and X. Obradors, *J. Phys. C: Solid State Phys.* **18,** L401 (1985).
5. H. M. Rietveld, *J. Appl. Crystallogr.* **2,** 65 (1969).
6. B. Toby, D. E. Cox, and P. Zolliker, unpublished work.
7. G. Blasse, *J. Inorg. Nucl. Chem.* **27,** 993 (1965).
8. E. O. Wollan and W. C. Koehler, *Phys. Rev.* **100,** 545 (1955).
9. R. E. Watson and A. J. Freeman, *Acta Crystallogr.* **14,** 27 (1961).
10. P. D. Battle, C. W. Jones, and F. Studer, *J. Solid State Chem.* **90,** 302 (1991).
11. T. C. Gibb, *J. Mater. Chem.* **2,** 415 (1992).
12. T. C. Gibb, *J. Chem. Soc. Dalton Trans.*, 2035 (1983).
13. P. D. Battle and C. W. Jones, *Mater. Res. Bull.* **22,** 1623 (1987).
14. M. Marezio and P. D. Dernier, *Mater. Res. Bull.* **6,** 23 (1971).
15. A. Vegas, M. Vallet-Regi, J. M. Gonzalez-Calbet, and M. A. Alario-Franco, *Acta Crystallogr. Sect. B* **42,** 167 (1986).
16. M. P. Attfield, P. D. Battle, S. K. Bollen, S. H. Kim, A. V. Powell, and M. Workman, *J. Solid State Chem.*, in press.
17. B. C. Tofield and B. E. F. Fender, *J. Phys. Chem.Solids* **31,** 2741 (1970).
18. W. C. Koehler and W. O. Wollen, *J. Phys. Chem. Solids* **2,** 100 (1957).
19. D. J. Breed, K. Gilijamse, J. W. F. Sterkenburg, and A. R. Miedema, *J. Appl. Phys.* **41,** 1267 (1970).
20. R. A. Cowley, *Philos. Trans. R. Soc. London Ser. B* **290,** 583 (1980).
21. R. A. Cowley, G. Shirane, R. J. Birgenau, E. C. Svensson, and H. J. Guggenheim, *Phys. Rev. B* **22,** 4412 (1980).
22. M. Cyrot, *Solid State Commun.* **39,** 1009 (1981).